

Apolipoprotein E•dipalmitoylphosphatidylcholine particles are ellipsoidal in solution[§]

Clare A. Peters-Libeu,* Yvonne Newhouse,* Steven C. Hall,^{†,§} H. Ewa Witkowska,^{†,§} and Karl H. Weisgraber^{1,*,**,††}

Gladstone Institute of Neurological Disease,* Biomolecular Resource Center Mass Spectrometry Facility,[†] Department of Cell and Tissue Biology,[§] Department of Pathology,^{**} and Cardiovascular Research Institute,^{††} University of California, San Francisco, CA 94158

Abstract Apolipoprotein E (apoE) is a major protein component of cholesterol-transporting lipoprotein particles in the central nervous system and in plasma. Polymorphisms of apoE are associated with cardiovascular disease and with a predisposition to Alzheimer's disease and other forms of neurodegeneration. For full biological activity, apoE must be bound to a lipoprotein particle. Complexes of apoE and phospholipid mimic many of these activities. In contrast to a widely accepted discoidal model of apoA-I bound to dimyristoylphosphatidylcholine, which is based on solution studies, an X-ray diffraction study of apoE bound to dipalmitoylphosphatidylcholine (DPPC) indicated that apoE•DPPC particles are quasi-spheroidal and that the packing of the phospholipid core is similar to a micelle. **§** Using small-angle X-ray scattering, we show that apoE•DPPC particles in solution are ellipsoidal and that the shape of the phospholipid core is compatible with a twisted-bilayer model. The proposed model is consistent with the results of mass spectrometric analysis of products of limited proteolysis. These revealed that the nonlipid-bound regions of apoE in the particle are consistent with an α -helical hairpin.—Peters-Libeu, C. A., Y. Newhouse, S. C. Hall, H. E. Witkowska, and K. H. Weisgraber. **Apolipoprotein E•dipalmitoylphosphatidylcholine particles are ellipsoidal in solution.** *J. Lipid Res.* 2007. 48: 1035–1044.

Supplementary key words lipoprotein • small-angle X-ray scattering • phospholipid • apolipoprotein A-I

Apolipoprotein E (apoE) is a protein component of lipoproteins in plasma and in the central nervous system (1). Small apoE-containing HDLs (~120 Å in diameter) are important for cholesterol transport in the central nervous system and plasma and participate in neuronal plasticity and repair (2). Model lipoproteins composed of apoE and phospholipid mimic many of the critical biological activities of naturally occurring apoE-containing lipoproteins, such as high-affinity binding to the LDL receptor and stimulation of cholesterol efflux from macrophages

(3, 4). ApoE4, a common isoform, is associated with an increased risk of neurodegenerative disease, including Alzheimer's disease (5). Rarer variants of apoE are associated with an increased risk of atherosclerosis due to a decreased binding affinity for heparin or the LDL receptor (6, 7).

ApoE is a member of a family of exchangeable apolipoproteins that includes apoA-I, the major structural apolipoprotein of plasma HDL particles. HDL particles containing apoA-I or apoE are antiatherogenic and are important mediators of reverse cholesterol transport (6). The amino acid sequence homology between apoE and apoA-I is 42%. Most of the homologous residues are located in their structurally similar N-terminal four-helix bundle domains (8, 9). In both proteins, the four-helix bundle must undergo a conformational change when the protein binds to lipid before it achieves its biologically active conformation (7, 10, 11). Although apoE and apoA-I are structurally similar in the lipid-free state, they have different effects on the size expansion of HDL that occurs with cholesterol loading during reverse cholesterol transport. ApoA-I is size limiting, whereas apoE promotes further size expansion (12), suggesting physiologically important differences in how the two proteins interact with lipid. Understanding the structure of biologically active model lipoprotein particles will be key to unraveling the mechanisms of the different physiological roles of apoA-I and apoE.

Although lipoproteins have been studied by electron microscopy, neutron scattering, and X-ray scattering, the limited resolution of these techniques has generally sufficed only for determining the shape of the particle and the radial distribution of electron density (as reviewed in Ref. 13).

Abbreviations: apo E, apolipoprotein E; DMPC, dimyristoylphosphatidylcholine; DPPC, dipalmitoylphosphatidylcholine; MS/MS, tandem mass spectrometry; ESI, electrospray ionization; POPC, 1-palmitoyl-2-oleoylphosphatidylcholine; SAXS, small-angle X-ray scattering.

¹To whom correspondence should be addressed.

e-mail: kweisgraber@gladstone.ucsf.edu

§The online version of this article (available at <http://www.jlr.org>) contains supplementary data in the form of a table.

Manuscript received 22 December 2006 and in revised form 15 February 2007.

Published, JLR Papers in Press, February 17, 2007.
DOI 10.1194/jlr.M600545-JLR200

Copyright © 2007 by the American Society for Biochemistry and Molecular Biology, Inc.

This article is available online at <http://www.jlr.org>

Originally, two structural models of lipoprotein particles were proposed. In one, the phospholipid is arranged in a micelle-like shape, with the protein partially submerged in the micelle surface. In the second, the discoidal model, the phospholipid is arranged as in a bilayer with the protein wrapped around the edge of the disk, covering the exposed hydrophobic tails of the phospholipid (14, 15).

Studies of apoA-I complexed with dimyristoylphosphatidylcholine (DMPC) by small-angle X-ray scattering (SAXS) and neutron scattering were limited by the computational difficulty of translating spherically averaged small-angle scattering data into a low-resolution model of the particle. As a result, only models consisting of concentric spherical shells or concentric cylindrical shells were tested against the data. The data best matched a cylindrical particle with a low-density inner core and a high-density outer ring. These studies concluded that the DMPC molecules were packed in a bilayer-type arrangement inside the cavity formed by a ring-like protein belt (~20 Å wide and 10 Å deep). The radius of the belt was estimated to be 45–49 Å with a height of 32.6–50 Å (16, 17). Subsequent biochemical and structural studies supported this conclusion, although the details of the folding of the apoA-I molecules within the belt varied (18). The discoidal model has been widely accepted for apoA-I-phospholipid complexes and has been applied to other apolipoprotein-phospholipid complexes (19).

However, in a recent X-ray crystallography study, we reached the surprising conclusion that the structure of particles composed of apoE and dipalmitoylphosphatidylcholine (DPPC) was similar to the micelle model (20). In the apoE•DPPC crystals, X-ray scattering due to the phospholipids was consistent with a spheroidal shape, in which the hydrophobic tails point toward the center of the particle and the phospholipid head groups are arranged on a spheroidal surface 60 Å in diameter. The apoE molecules appeared to be folded into a discrete horseshoe shape that primarily interacted with the polar head groups of the phospholipid. However, the crystallization of the particles could potentially influence their shape.

In this study, SAXS was used to analyze apoE•DPPC and apoA-I•DMPC particles and to determine their shape in solution. We compared the radius of gyration, maximum dimension, and the pair distribution function from the SAXS measurements with the predictions of the X-ray model. We also used a phase-contrast method to determine the relative molecular volumes of protein and phospholipid and the maximum dimension of the internal cavity containing the acyl chains of the phospholipid. We conclude that the parameters derived from the SAXS measurements for the apoE•DPPC particles are consistent with the predictions of the X-ray model, confirming that the apoE•DPPC particles are not discoidal in solution.

MATERIALS AND METHODS

Protein and lipoprotein particle purifications

Recombinant apoE4 was expressed and purified as described (21), and apoE4•DPPC particles were produced as described

(22). However, the high transition temperature of DPPC requires the addition of cholate to produce lipoprotein particles, and its removal might affect particle morphology. Therefore, to determine whether the cholate removal method affects morphology, apoE•DPPC particles were produced by two different methods. In the first, cholate was removed with an anion exchange resin (Biobeads), and the particles were purified by size-exclusion chromatography, as described (22). In the second, cholate was removed by extensive dialysis followed by centrifugation against a potassium bromide gradient.

Recombinant human apoA-I protein was expressed and purified as described (23). ApoA-I•DMPC particles were made by combining purified apoA-I with dispersed DMPC at a 1:1 mass ratio in 10 mM Tris, pH 8.0, and 100 mM sodium chloride, as described (24), and purified by size-exclusion chromatography.

SAXS

SAXS data were collected at beamline 12.3.1 at the Advanced Light Source using an X-ray wavelength of 1.115 Å and particle concentrations of 0.7–4.5 mg/ml. The data were integrated with custom software, and pair distribution functions were calculated with the program GNOM (25) except for the data in 0.359 eÅ^{-3} buffer for apoA-I•DMPC. Addition of sucrose beyond 300 mM (0.347 eÅ^{-3}) for apoA-I•DMPC promoted dimerization of the particles. The radius of gyration for the monomer was determined using Guinier analysis to separate the contributions of the dimer (radius of gyration ~140 Å) and the monomer (radius of gyration ~73 Å). To calculate the representative pair distribution function for the monomer, data points in the Guinier region of the dimer (the first 15 points out of 450) were eliminated from the curve before the use of GNOM. The resulting radius of gyration for this pair distribution function ($72 \pm 1 \text{ Å}$) was in good agreement with the radius of gyration estimated from Guinier analysis.

For calculations of scattering curves, the protein model was generated by placing helices in the low-resolution molecular envelope derived from the X-ray diffraction study (20). In this calculation, the relative positions of the helices in the model function as placeholders so that correct average electron density is placed in the appropriate volume. Several alternate models were constructed to account for the scattering mass of residues outside the molecular envelope. Their positions were determined by comparison with ab initio models calculated with the program DAMMIN (26). The scattering curves for the protein models were calculated with CRY SOL (27), and the relative positions of the molecules were refined with MASHA (28).

The model to fit the data was derived from the crystal structure of $\Delta 43$ apoA-I (29). Alignment of the molecular envelope with sections of the ring-like configuration of the apoA-I molecule indicated that the molecular envelope could be filled with two sections of adjacent apoA-I molecules in a manner that accounted for 275 of the 299 residues of apoE. Only minor adjustments of the apoA-I protein were required to match the curvature of the molecular envelope. Alignment of the apoE and apoA-I sequences suggested that the best alignment could be obtained by excluding the first 24 N-terminal residues. These residues were modeled as a long extension, using the ab initio models as a guide.

Limited proteolysis

Accessible loops in the apoE•DPPC particles were identified by limited proteolysis. ApoE4•DPPC (100 µg) was incubated in 10 mM Tris, pH 7.4, and 150 mM sodium chloride (TBS) buffer with endoproteinase Glu-C, trypsin, and elastase (enzyme:substrate ratio, 1:100; reaction volume, 100 µl) for 10 min at room

temperature. The digestion was stopped with 1 μl of neat formic acid. Aliquots (10 μl) were dried on a speedvac, solubilized in 10% acetonitrile-0.2% formic acid, dried again, and then reconstituted in 10 μl of 50% acetonitrile-0.1% formic acid. Typically, 3 μl samples were loaded into NanoES spray capillaries (Proxeon Biosystems) for direct infusion into the mass spectrometer. Electrospray ionization (ESI) MS and tandem mass spectrometry (MS/MS) analyses were performed using a QqTOF mass spectrometer (QSTAR XL, Applied Biosystems/MDS Sciex) equipped with a nanospray ion source (Protana). Nitrogen was used as the collision gas. The collision energy for MS/MS experiments was manually adjusted to the level that afforded precursor ion intensity at 30–50% of its initial value. Spectra were deconvoluted to a zero-charge state using Bayesian Protein and Peptide Reconstruct tools (Applied Biosystems/MDS Sciex). FindPept tool (<http://ca.expasy.org/tools/findpept.html>) and Protein Prospector MS-product tool (<http://prospector.ucsf.edu/ucsfhtml4.0/msprod.html>) were used to manually match experimental masses of intact proteolytic fragments and product ions derived from them during the process of MS/MS, to the theoretical values based on the sequence of apoE4.

RESULTS

Comparison of apoE•DPPC particles purified by two different methods

The SAXS profiles for apoE•DPPC particles produced by removing cholate using either anion exchange or dialysis were nearly identical (Fig. 1), suggesting that the morphology of the particles is determined by the initial phospholipid:protein:cholate ratio rather than by the purification method. The small differences in the SAXS profiles probably reflect differences in the polydispersity of the particles, as shown by Guinier plots (Fig. 1A, inset). A Guinier plot is related to the polydispersity of particles in solution, with a linear plot indicating a solution with a single species and curvature indicating a mixture of species (30). Particles produced with the dialysis method had a better fit to the linear model than those produced with the anion exchange method (correlation coefficient 0.98 vs. 0.93). Thus, apoE•DPPC particles made with the dialysis method are less polydisperse and can be treated as a monodisperse solution. We therefore used the dialysis method to produce apoE•DPPC particles for further analysis.

Comparison of apoE•DPPC and apoA-I•DMPC particles

The radius of gyration and the maximum dimensions of the apoE•DPPC particles were similar to those of apoA-I•DMPC particles (Table 1); however, the SAXS curves at low scattering angles differed considerably (Fig. 1B, C), indicating very differently shaped particles. In addition, the change in the X-ray scattering as the electron density of the solvent increased indicated that the distribution of the protein and the phospholipid within the two particles is very different.

The pair distribution functions of apoA-I•DMPC particles (Fig. 2A) were consistent with a discoidal model and very similar to previously published pair distribution functions (17) and those of DPPC nanodiscs of scaffolding

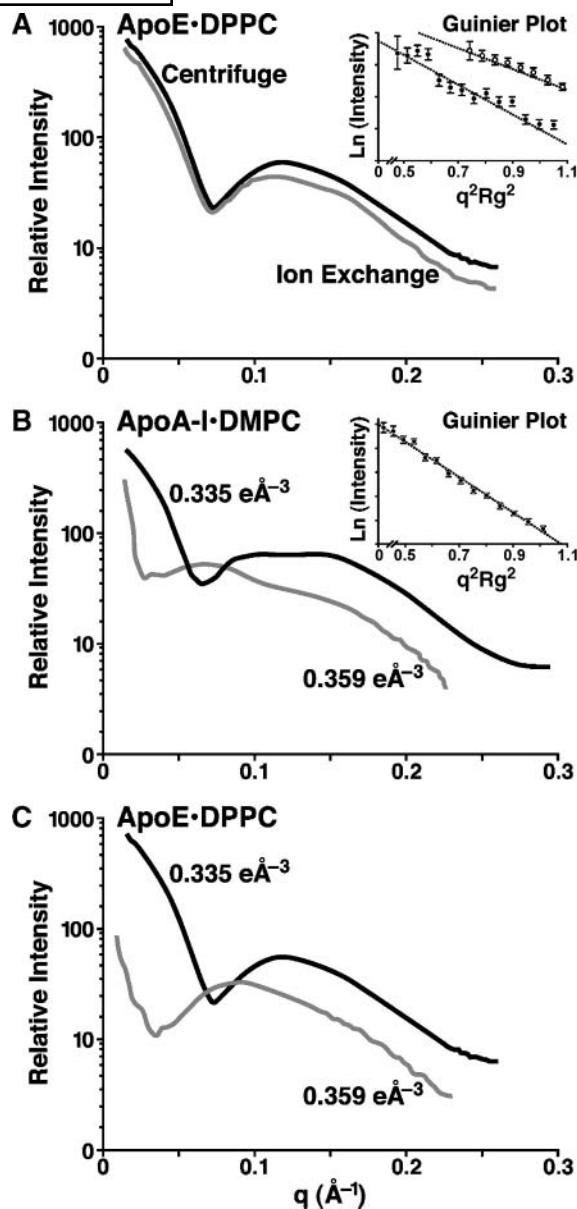


Fig. 1. Comparison of the small-angle X-ray scattering (SAXS) profiles of apolipoprotein E (apoE)•dipalmitoylphosphatidylcholine (DPPC) and apoA-I•dimyristoylphosphatidylcholine (DMPC). A: apoE•DPPC particles in 0.335 $\text{e}\text{\AA}^{-3}$ buffer prepared using two different methods. The magnitude of the scattering vector (q) is in units of $4\pi\sin(\theta)/\lambda$, where θ is the scattering angle and λ is the wavelength. Inset shows the corresponding Guinier plots for the ion exchange method (closed circles) and the centrifuge method (open circles). B: ApoA-I•DMPC in buffer with an electron density of 0.335 (black) and 0.359 $\text{e}\text{\AA}^{-3}$ (gray). Inset shows a Guinier plot for apoA-I•DMPC in 0.335 $\text{e}\text{\AA}^{-3}$ buffer. C: ApoE•DPPC particles prepared using the centrifuge method in buffer with an electron density of 0.335 (black) or 0.359 (gray) $\text{e}\text{\AA}^{-3}$.

proteins similar to apoA-I (31). The two negative peaks in the pair distribution function measured in high electron density buffer are thought to result from the unequal distribution of electron density in the phospholipid bilayer. In a bilayer, the less-dense hydrophobic tails of the DMPC are packed in pools approximately 10–15 \AA wide between

TABLE 1. Radius of gyration and dimensions of the apoE•DPPC and apoA-I•DMPC particles

Lipoprotein Particle	R_g (Å)	Maximum Dimension (Å)
ApoE•DPPC (anion exchange)	46.36 ± 0.07	130 ± 5
ApoE•DPPC (dialysis)	45.89 ± 0.08	130 ± 5
Human apoA-I•DMPC	49.41 ± 0.04	130 ± 5
Porcine apoA-I•DMPC	49 (17)	N/A

ApoE, apolipoprotein E; DMPC, dimyristoylphosphatidylcholine; DPPC, dipalmitoylphosphatidylcholine; R_g , radius of gyration.

the tightly clustered methylene groups in the center and the more electron-dense phospholipid head groups at the periphery. For DMPC and DPPC at room temperature, the approximate spacing between these pools in the two leaflets of the bilayer is 25–30 Å (32), which gives rise to the negative peak near 30 Å. In buffers with even higher electron density, a second negative peak appears in the pair distribution function, because most of the atoms within the interior of each leaflet of the bilayer are in regions with a lower electron density than the buffer.

In contrast, the apoE•DPPC pair distribution function in TBS or 10% sucrose does not display this characteristic signature of a phospholipid bilayer; instead, the negative region is broad, extending to 60 Å, and roughly symmetrical (Fig. 2B). Therefore, the pair distribution functions for the apoE•DPPC particles support the conclusions from the X-ray diffraction experiments that the DPPC does not form a bilayer in the particles and that the majority of the phospholipids are confined within a volume

approximately 60 Å in diameter. The symmetry of the negative peak in the apoE•DPPC particle indicates that the volume is almost spherically symmetrical after rotational averaging.

Agreement of the X-ray model with the SAXS data

To directly test the agreement of the X-ray model with the SAXS data, the SAXS profiles of the apoE•DPPC particles were measured at four different contrasts produced by varying the electron density of the buffer with sucrose. The method of Moore, Engelman, and Schoenborn (33) was used to calculate the molecular volumes of the apoE and the DPPC and their radii of gyration (see supplementary Table II) and to determine whether the apoE•DPPC particles are cylindrically or spherically symmetrical.

As predicted by the X-ray model, analysis of the dependence of the apparent radius of gyration on the fraction of scattering due to the phospholipids indicated that the protein within the apoE•DPPC particles is not distributed in a cylindrically or spherically symmetrical fashion. In a symmetrical particle, the center of mass of the protein should coincide with the center of mass of the DPPC and the center of mass of the particle, as predicted by Moore, Engelman, and Schoenborn (33). In this case, the apparent radius of gyration of the particles is a linear function of the fraction of scattering due to the phospholipids as for the apoA-I•DMPC particles (Fig. 3) (17). In these particles, both the protein and the DMPC are thought to be contained in cylindrically symmetric belts. In contrast, for apoE•DPPC particles, the apparent radius of gyration was fit by a quadratic function of the fraction of the scattering due to the phospholipids. As described by Moore, Engelman, and Schoenborn, this quadratic function results

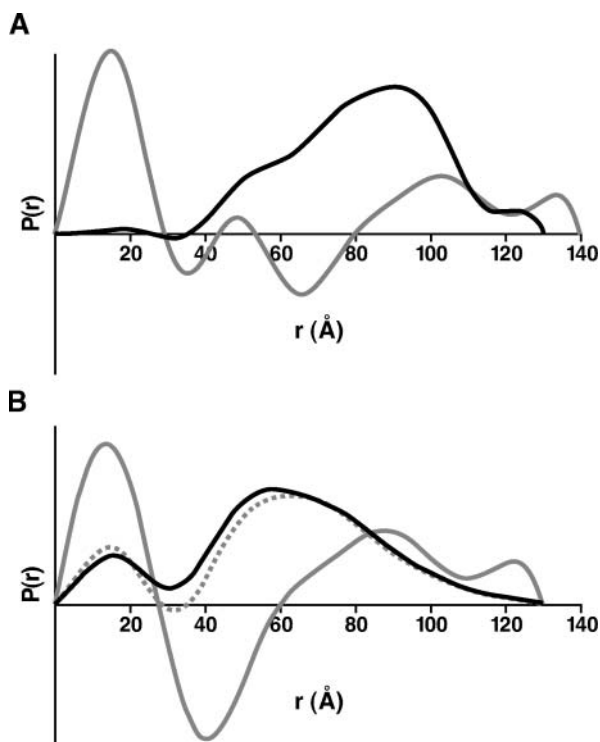


Fig. 2. Distance distribution functions. A: ApoA-I•DMPC in 0.335 (black) and 0.359 (gray) $e\text{Å}^{-3}$ buffer. B: ApoE•DPPC in 0.335 (black), 0.339 (dashed gray), and 0.359 $e\text{Å}^{-3}$ (gray) buffer.

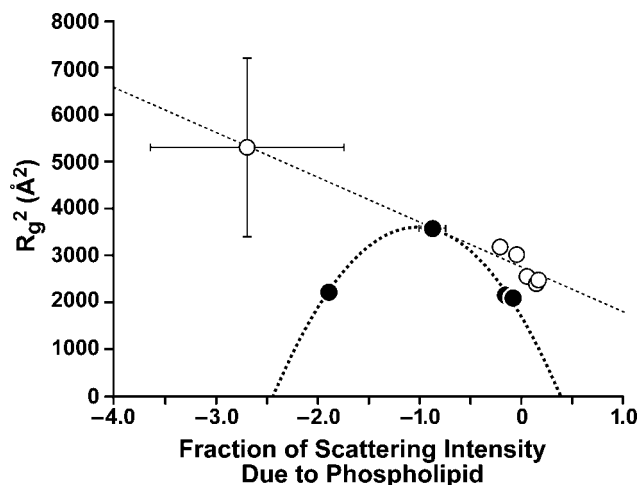


Fig. 3. Effect of contrast on the radius of gyration squared for apoE•DPPC (closed circles) and apoA-I•DMPC (open circles). The fraction of the scattering intensity due to the phospholipid was calculated using an average electron density of $0.34 e\text{Å}^{-3}$ for DMPC, $0.33 e\text{Å}^{-3}$ for DPPC, $0.42 e\text{Å}^{-3}$ for apoA-I, and $0.45 e\text{Å}^{-3}$ for apoE. These values were estimated from the contrast data as described in Supplementary Material online. For the points shown without error bars, the estimated error is less than the size of the symbol.

from an asymmetric distribution of electron density within the particles that causes the center of mass of the protein not to coincide with the center of mass of the phospholipid or the particle. The X-ray model of apoE•DPPC falls into this case because the protein is contained in two nonintersecting volumes.

In addition to testing the symmetry of the protein distribution within the particle, we used contrast variation to estimate the volumes and radii of gyration of the apoE and DPPC molecules. The molecular volume of apoE and its radius of gyration agreed closely with the X-ray model (Table 2). However, the estimated radius of gyration of the DPPC was significantly larger than that calculated for a spherical volume. This independent estimate of the size of the lipid pool indicates that the DPPC molecules in the apoE•DPPC particles are distributed in a more ellipsoidal volume than suggested by the X-ray model.

Refinement of the apoE•DPPC model

The more ellipsoidal volume can be independently tested by refining the positions of the apoE molecules from the X-ray model against the SAXS data. Because the electron density of the TBS buffer ($0.335 \text{ e}\text{\AA}^{-3}$) is quite close to that of the phospholipid ($0.331 \text{ e}\text{\AA}^{-3}$) (Supplemental Material), the scattering curve in TBS is dominated by scattering from the much more electron-dense protein. Therefore, the positions of the apoE molecules were subjected to rigid body refinement against the SAXS profile (200–20 Å) of the particles in TBS using the program MASHA (28). For the SAXS data (50–20 Å) that overlap the X-ray data, refinement of the relative position of the protein molecules substantially increased the fit of the calculated scattering profile (Fig. 4A) and resulted in an ellipsoidal volume between the two apoE molecules (Fig. 4B).

Limited proteolysis of apoE•DPPC

Because the degree of superhelical twisting of the hairpin contributes to the scattering profile in the higher-

TABLE 2. Model parameters derived from SAXS contrast data and X-ray crystallography

	SAXS Contrast ^a	X-ray Crystallography	Refined SAXS
Specific volume of apoE molecule (10^4 \AA^3)	3.95 ± 0.05	3.9 ± 0.3	3.7
R_g of protein (Å)	40.4 ± 1.5	40.8 ± 4	40.6
R_g of DPPC (Å)	42.0 ± 2.0	$23 - 37^b$	$32-43^b$

SAXS, small-angle X-ray scattering; The errors indicated for the X-ray crystallography model were estimated from comparison of models in which the R-factor for molecular replacement was <0.48.

^aThis calculation is explained in detail in the Supplementary Material.

^bThe phospholipids are modeled as two distinct shells: an inner shell with a radius of 26 Å and an outer shell with a minimum radius of 32 Å, which increases to the maximum radius of the protein when near the molecular envelope. The minimum R_g is calculated assuming that the contrast of the shells is equal. The maximum R_g is calculated assuming that the contrast of the outer shell is twice the contrast of the inner shell.

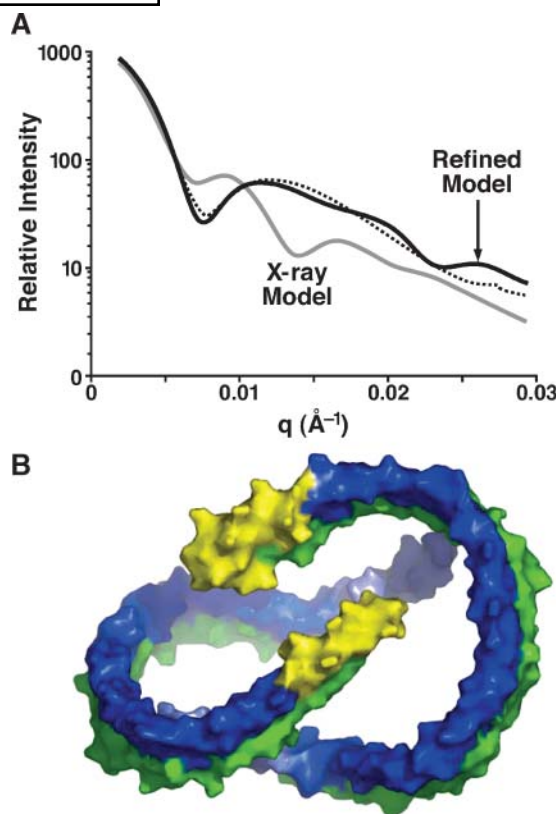


Fig. 4. Refinement of the X-ray model. A: Comparison of the model derived from X-ray diffraction analysis of the apoE•DPPC crystals with the SAXS data at $0.335 \text{ e}\text{\AA}^{-3}$ (black). The calculated scattering from the X-ray model is shown as a dashed gray line. The calculated scattering from the refined SAXS model is shown as a solid gray line. B: Protein envelope derived from the refined SAXS model. The volume assigned to the NH_2 -terminal domain is colored blue. The COOH -terminal domain is colored green, and yellow marks the volume that may contain the LDL-receptor binding site.

resolution range, the fit to the SAXS profile was improved further by testing various possible hairpin models based on known crystal structures. To further constrain the model building, limited proteolysis coupled with mass spectrometry was used to identify primary cleavage sites. ApoE4•DPPC was incubated with three different proteolytic enzymes (trypsin, endoproteinase Glu-C, and elastase) and the resulting oligopeptides were analyzed by ESI MS and MS/MS without any separation.

ESI MS of products of apoE4 digestion with Glu-C and elastase were dominated by multiply charged ions representing large oligopeptides. Fully digested peptides constituted a minor component in both samples, as judged by the relative intensities of their corresponding molecular ions. In contrast, tryptic digestion produced only one large oligopeptide accompanied by a significant number of fully proteolyzed peptides. The molecular masses and identities of large oligopeptides detected in all three digests are shown in Table 3.

The identities of proteolytic fragments were proposed on the basis of manual matching of experimental aver-

TABLE 3. Mass spectrometric analysis of products of limited proteolytic digestion of apoE•DPPC

Enzyme	Experimental Mass ^a (Da)	Theoretical Mr	Mass Error (Da)	Sequence Assignment ^b	MS/MS
Glu-C	1,9353.5	19,354.9	-1.4	(E) 14L→168E (G)	Yes
Glu-C	18,213.2	18,214.7	-1.5	(E) 14L→179E (R)	Yes
Glu-C	8,958.9	8,960.1	-1.2	(E) 221M→299H ()	Yes
Trypsin	9,032.2	9,033.1	-0.9	[R] 16Q→90R (A)	Yes
Elastase	20,495.0	20,497.1	-2.1	(<i>)GS</i> 1K→175S (A)	No
Elastase	22,468.5	22,470.4	-1.9	(<i>)GS</i> 1K→193A (T)	No
Elastase	34,295.1	34,296.7	-1.6	(<i>)GS</i> 1K→298N (H)	No
Elastase	22,326.4	22,328.3	-1.9	(<i>)GS</i> 1K→191R (A) ^c	Yes
Elastase	11,005.8	11,007.5	-1.7	(A) 194T→289T (S)	No
Elastase	11,234.2	11,236.7	-2.5	(A) 194T→292A (P) ^d	No
Elastase	11,844.8	11,846.3	-1.5	(A) 194T→298N (H)	No
Elastase	11,981.6	11,983.5	-1.9	(A) 194T→299H ()	No

MS/MS, tandem mass spectrometry.

^aExperimental average molecular mass calculated by deconvoluting multiply charged molecular ions to a zero-charge state species.

^bRecombinant apoE4 carried GS at the N-terminus. These first two amino acid residues are not included in sequence numbering and are shown in italics. Amino acid residues flanking cleavage sites are shown in parentheses; empty parentheses () indicates a proteolytic fragment that originates at the N-terminus or terminates at the C-terminus.

^cProbably a secondary product derived from peptide [*()GS* 1K→193A (T)] by removal of two C-terminal alanines.

^dElastase cleavage before proline was observed previously (43).

age molecular masses to the theoretical *in silico*-derived values. The following criteria were used to select between candidates of very similar molecular masses: consistency in mass measurement (same level of mass error), use of a minimal number of cleavage sites to explain the observed proteolytic fingerprint, and the typically observed enzyme specificity. MS/MS analysis was used to confirm the identities of some of the proteolytic fragments. In each case, an abundance of product ions was detected that allowed for unequivocal assignment of proteolytic fragment identity.

Figure 5 illustrates MS/MS data acquired for oligopeptide 14L→168E (generated from apoE4 during digestion with Glu-C). A molecular ion carrying 17 positive charges was used as a precursor in this analysis. Mass spectrometric analysis of products of limited proteolysis of apoE4 identified the following cleavage sites: E13, R15, R90, E168, S175, E179, R191, A193, E220, T289, A292, and N298. The presence of families of proteolytic fragments of different lengths sharing one of the termini, such as the Glu-C fragments with NH₂-termini at E13 or elastase fragments with N-termini at T194, introduces the possibility of a secondary processing of the initially produced larger fragments. For fragments in the NH₂-terminal domain, the known secondary structure can be used as a guide. For example, the secondary structure in the nonlipidated form of the NH₂-terminal domain of R61 mouse apoE suggests that the E168 and E179 Glu-C fragments may be independent, because both of these residues occur in flexible loops (34). In contrast, S175 is in the middle of an α -helix, which suggests that the S175 elastase fragment may result from secondary processing of the A193 fragment.

With these limitations in mind, we propose that the sites that represent the most likely primary sites are E13, R15, R90, E168, E179, A193, and E220. This pattern of proteolytic sites is consistent with an α -helical hairpin

model, because the sites are from both domains. In addition, the two NH₂-terminal sites are consistent with the assignment of the extension from the X-ray hairpin envelope to residues 1–20 of the NH₂-terminal domain. Inclusion of this extension was suggested by *ab initio* models of the protein envelope obtained using DAMMIN (26). Addition of this extension greatly improved the fit of the model to the small-angle scattering curve.

Agreement of X-ray model with final SAXS model

The refined SAXS models were in good agreement with the X-ray model, given the resolution of the two techniques. The change in the relative displacements of the apoE molecules is relatively modest for a low-resolution model. The distance between the center of mass of the apoE molecules increases from 26 Å to 37 Å. Although the changes appear large, because of the low resolution of the X-ray model and the lack of very low resolution reflections in the X-ray diffraction data set, these displacements are well within the error of the original model. A much larger change occurs in the relative orientation of the two molecules. The rigid body refinement rotated one of the apoE molecules so that the medial planes of the apoE molecules were nearly perpendicular to each other. In the original X-ray model, the angle between these planes resulted from a crystallographic symmetry operation. Therefore, as with the intermolecular distance, some of the difference in the relative orientation of the apoE molecules in the two techniques can be explained by errors in the placement of the apoE molecule within the crystal lattice. Although rigid body refinement of the apoE molecules with the SAXS data results in a slightly larger particle than the original X-ray model, the overall shape of the two apoE molecules derived from the X-ray diffraction study is an excellent match for the SAXS data, considering that this calculation neglects the small contribution from the phospholipid. The larger particle dimen-

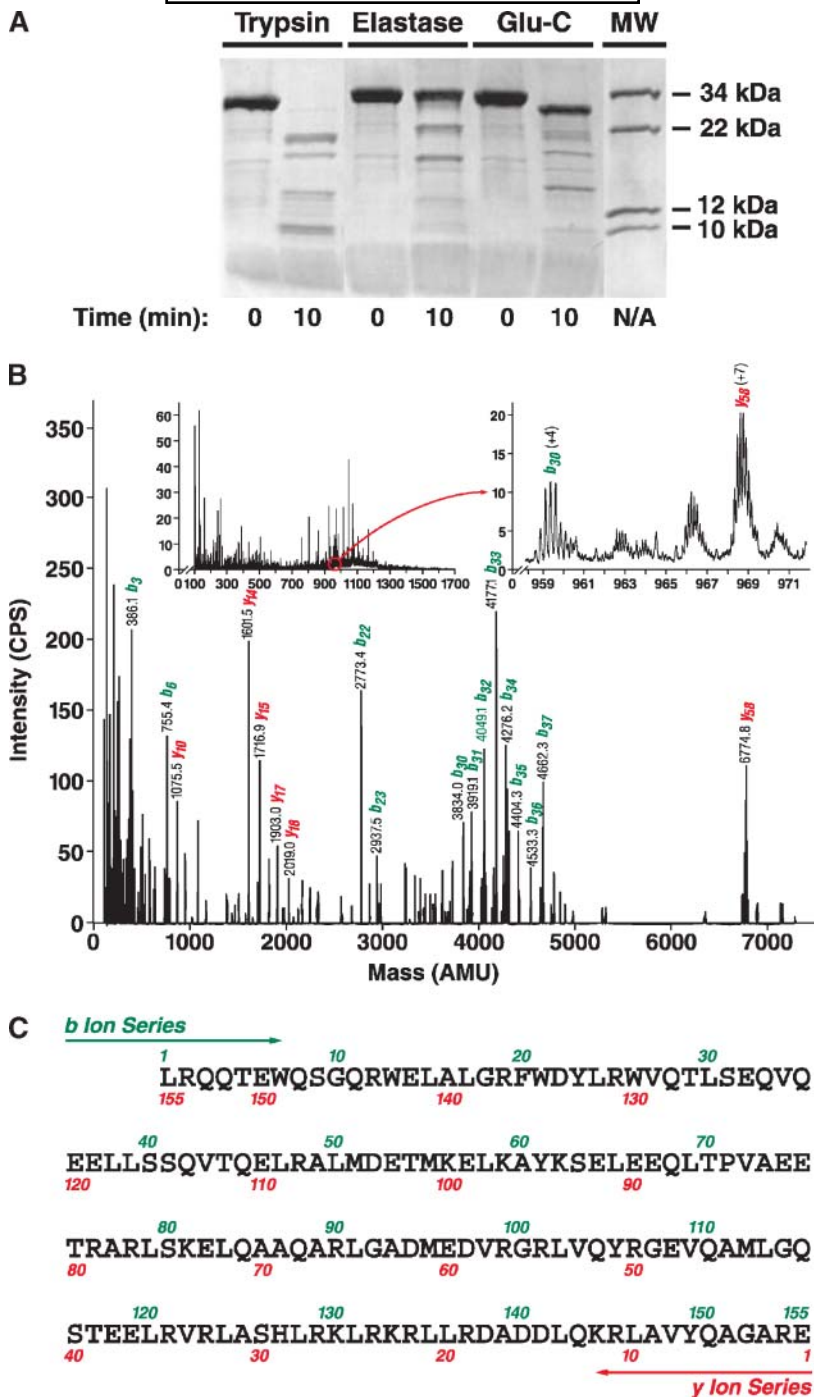


Fig. 5. Analysis of products of limited proteolysis of apoE•DPPC. **A:** SDS PAGE showing the products of limited digestion of apoE•DPPC with trypsin, elastase, and Glu-C. The molecular weight markers (MW) are a mixture of full-length apoE and its 22-kDa, 12-kDa, and 10-kDa thrombin fragments. **B:** Tandem mass spectrometry (MS/MS) spectra of the Glu-C proteolytic fragment 14L→168E (Mr 18,214.7). The zero-charge state electrospray ionization (ESI) MS/MS spectrum of precursor ion m/z 1,072.5 (+17 charge state) depicted in the panel was reconstructed from raw data shown in the top left inset; the top right inset shows the zoomed portion of the raw MS/MS spectrum illustrating typical mass resolution of multiply charged product ions. Many intense product ions are derived from cleavages after aspartate (y_{14} , y_{15} , y_{58} , b_{22}). However, the major product ion-cluster, represented by a series of b ions (b_{30} – b_{36}), is derived from the region 40 VQTLSEQVQ 49 E that is devoid of any obvious gas-phase fragmentation-enhancing features. The same fragmentation pattern was observed for precursor ions m/z 1,215.4 (+15), 1,013.0 (+18) and 959.7 (+19) (data not shown). Likewise, the related Glu-C proteolytic fragment encompassing 14L→179E produced pronounced gas-phase cleavages within the same 40V→49E section of the molecule for precursor ions m/z 968.7 (+20) and 1,019.8 (+19), as did the elastase-generated proteolytic fragment [GS 1K→191R] for precursor ion 1,015.8 (+22) (data not shown). **C:** Annotated sequence of the Glu-C proteolytic fragment 14L→168E (Mr 18,214.7). Numbers shown above and below the amino acid sequence refer to a system of annotation for b series and y series product ions that are generated in the gas phase in the course of collision-induced dissociation of an oligopeptide at peptide bonds.

sion is consistent with the large radius of gyration derived independently for the phospholipid in solution from the contrast variation data (Table 2).

Because apoE•DPPC particles are flexible in solution, the relative orientation of the apoE molecules and the distribution of the phospholipid may vary throughout the population in solution. The SAXS data reflect an average over the entire population of apoE•DPPC particles in solution. The larger, more ellipsoidal particle shape resulting from the SAXS analysis may reflect a broader population of particles than are present in the crystal. In this view, crystallization may have selected a subpopulation of smaller particles for incorporation into the lattice. A second possibility is that high concentrations of polyethylene glycol 1000 (PEG 1000) or low pH in the crystallization buffer may have caused some minor remodeling of the particles. More-extensive remodeling of apoA-I•DMPC particles has been observed with higher-molecular-weight PEGs (35). However, particles from dissolved apoE•DPPC crystals have an electrophoretic mobility identical to that of native apoE•DPPC crystals under nondenaturing conditions, ruling out any large changes in particle morphology (22).

DISCUSSION

Models of the apoE•DPPC particle in solution

To explore further the potential shape of the apoE•DPPC particles, we generated models of the phospholipid

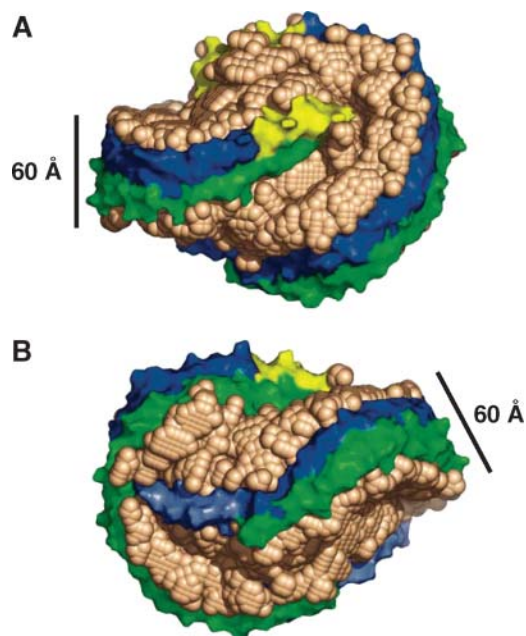


Fig. 6. A twisted-bilayer model of apoE•DPPC. In the molecular envelope of the apoE molecule, blue indicates the NH₂-terminal domain, green the COOH-terminal domain, and yellow marks the volume that may contain the LDL receptor binding site. The minimal volume of the phospholipid is filled by the tan balls. A: Edge-on view of the envelope of an apoE molecule. B: Ninety-degree rotation of the molecule about a horizontal axis.

volume by placing balls in the cavity formed by the refined SAXS model of the apoE molecules. The model shown in **Fig. 6** was generated by restricting the phospholipid volume to a maximal dimension of 60 Å in directions perpendicular to the central plane of the protein model. The distribution of the balls was constrained so that it could only deviate from a 60-Å sphere when close to the protein and defines the minimal volume that gives a radius of gyration of 43 Å for the phospholipid. This model is remarkably similar to the models of apoA-I•1-palmitoyl-2-oleoylphosphatidylcholine (POPC) derived from molecular dynamics simulations (36) in which the POPC bilayers are twisted. The minimal volume for the DPPC derived from the SAXS analysis clearly suggests that a twisted DPPC bilayer is a possible model for the apoE•DPPC particles in solution.


Although our data indicate that the DPPC is not packed in a highly ordered bilayer, the twisting of the DPPC so that the two parts of the bilayers are nearly perpendicular angles results in a model that, when rotationally averaged, is consistent with the symmetrical negative peaks seen in the SAXS analysis of apoE•DPPC particles at high contrast. Twisting of the bilayer presumably results in large distortions of its internal structure and a more even distribution of low-electron-density regions after rotational averaging.

The twisted-bilayer model also suggests that the DPPC in the particles can have bilayer-like subdomains with substantially different orientations in the interior of the particle, consistent with the strong diffuse scattering centered at 4.2 Å observed in the crystals. This is consistent with a recent structural analysis of much larger apoE•DMPC particles by calorimetry and internal reflection infrared spectroscopy (37). That analysis indicated that some of the apoE helices were perpendicular and some parallel to the acyl chains of the phospholipids, in contrast to the disc model, where the protein helices have only one orientation.

The SAXS data are an average over the population of particles and their conformational states in solution. Therefore, our twisted-bilayer model reflects the ensemble average of the particles in solution and suggests that the apoE-containing particles are much more dynamic in solution than previously thought. This flexibility is due to the fact that apoE folds into autonomous molecules that can move independently in the particle, a property that originates in sequence differences between apoE and apoA-I. Comparison of the apoE and apoA-I sequences indicates that apoE has fewer hydrophobic residues and suggests that there are more potential sites of interaction with the phospholipid head groups. ApoE is unusually rich in arginines (11% vs. 4.2% for all vertebrate proteins) (38), and has twice as many as apoA-I (34 of 299 vs. 17 of 242 residues). Indeed, the original name for apoE was arginine-rich protein (39). High levels of arginine are commonly found in proteins that bind phosphate or phosphate-rich ligands such as DNA or RNA, reflecting the highly favorable binding energy between arginine and phosphate. For example, in proteins that specifically bind

phospho-amino acids, the phospho-amino acid is commonly coordinated by a pair of arginines that have been polarized through their participation in a hydrogen network with nearby acidic residues (40). The 17 conserved arginines in apoE between residues 90 and 233 form seven clusters of two to four arginines that project from the same helical face, with at least one arginine in the cluster adjacent to an aspartate or a glutamate. In contrast, apoA-I has two such clusters of four arginines within the entire sequence.

This overall pattern of clusters of basic and acidic residues on the same face of the amphipathic helices in apolipoproteins has long been recognized as a potential binding site for the polar head groups of phospholipids (41). This hypothesis has been supported by the observation of this type of interaction between polarized lysines in apoC-II and the phosphate atoms in dodecylphosphorylcholine (42). The clusters in apoE can be modeled to form similar phosphate binding sites on the surface of the apoE hairpin. This analysis suggests that interactions between the polar residues in apoE and the phospholipid head groups contribute more to particle stability and overall particle structure than in lipoprotein particles containing apoA-I.

In summary, SAXS analysis indicated that apoE•DPPC particles are ellipsoidal with a spheroidal internal cavity. These results indicate that although apoE and apoA-I are structurally homologous in the lipid-free form, the two proteins combine with phospholipids to form particles with very different morphologies. 

This work was supported in part by Grant HL-64963 from the National Institutes of Health (to K.H.W.). Portions of this research were carried out through the general user program of the Advanced Light Source. The Biomolecular Resource Center Mass Spectrometry Facility acknowledges support from the Sandler Family Foundation. The authors thank Dr. Greg Hura for assistance with the small-angle scattering measurements, Dr. Sissel Lund-Katz for the apoA-I expression vector, Stephen Ordway and Gary Howard for editorial assistance, Karina Fantillo for manuscript preparation, and John Carroll for graphics assistance.

REFERENCES

- Mahley, R. W., and Y. Huang. 1999. Apolipoprotein E: from atherosclerosis to Alzheimer's disease and beyond. *Curr. Opin. Lipidol.* **10**: 207–217.
- Mahley, R. W., and S. C. Rall, Jr. 2000. Apolipoprotein E: far more than a lipid transport protein. *Annu. Rev. Genomics Hum. Genet.* **1**: 507–537.
- Pitas, R. E., T. L. Innerarity, and R. W. Mahley. 1980. Cell surface receptor binding of phospholipid-protein complexes containing different ratios of receptor-active and -inactive E apoprotein. *J. Biol. Chem.* **255**: 5454–5460.
- Koo, C., T. L. Innerarity, and R. W. Mahley. 1985. Obligatory role of cholesterol and apolipoprotein E in the formation of large cholesterol-enriched and receptor-active high density lipoproteins. *J. Biol. Chem.* **260**: 11934–11943.
- Saunders, A. M., W. J. Strittmatter, D. Schmechel, P. H. St George-Hyslop, M. A. Pericak-Vance, S. H. Joo, B. L. Rosi, J. F. Gusella, D. R. Crapper-MacLachlan, M. J. Alberts, et al. 1993. Association of

- apolipoprotein E allele $\epsilon 4$ with late-onset familial and sporadic Alzheimer's disease. *Neurology.* **43**: 1467–1472.
- Mahley, R. W. 2001. Biochemistry and physiology of lipid and lipoprotein metabolism. In *Principles and Practice of Endocrinology and Metabolism*. 3rd edition. K. L. Becker, editor. Lippincott Williams & Wilkins, Philadelphia. 1503–1513.
- Weisgraber, K. H. 1994. Apolipoprotein E: structure–function relationships. *Adv. Protein Chem.* **45**: 249–302.
- Wilson, C., M. R. Wardell, K. H. Weisgraber, R. W. Mahley, and D. A. Agard. 1991. Three-dimensional structure of the LDL receptor-binding domain of human apolipoprotein E. *Science.* **252**: 1817–1822.
- Ajees, A. A., G. M. Anantharamaiah, V. K. Mishra, M. M. Hussain, and H. M. K. Murthy. 2006. Crystal structure of human apolipoprotein A-I: insights into its protective effect against cardiovascular diseases. *Proc. Natl. Acad. Sci. USA.* **103**: 2126–2131.
- Lu, B., J. A. Morrow, and K. H. Weisgraber. 2000. Conformational reorganization of the four-helix bundle of human apolipoprotein E in binding to phospholipid. *J. Biol. Chem.* **275**: 20775–20781.
- Hatters, D. M., C. A. Peters-Libeu, and K. H. Weisgraber. 2006. Apolipoprotein E structure: insights into function. *Trends Biochem. Sci.* **31**: 445–454.
- Mahley, R. W., Y. Huang, and K. H. Weisgraber. 2006. Putting cholesterol in its place: apoE and reverse cholesterol transport. *J. Clin. Invest.* **116**: 1226–1229.
- Segrest, J. P., M. K. Jones, H. De Loof, and N. Dashti. 2001. Structure of apolipoprotein B-100 in low density lipoproteins. *J. Lipid Res.* **42**: 1346–1367.
- Tall, A. R., D. M. Small, R. J. Deckelbaum, and G. G. Shipley. 1977. Structure and thermodynamic properties of high density lipoprotein recombinants. *J. Biol. Chem.* **252**: 4701–4711.
- Assmann, G., and H. B. Brewer, Jr. 1974. A molecular model of high density lipoproteins. *Proc. Natl. Acad. Sci. USA.* **71**: 1534–1538.
- Wlodawer, A., J. P. Segrest, B. H. Chung, R. Chiovetti, Jr., and J. N. Weinstein. 1979. High-density lipoprotein recombinants: evidence for a bicycle tire micelle structure obtained by neutron scattering and electron microscopy. *FEBS Lett.* **104**: 231–235.
- Atkinson, D., and G. G. Shipley. 1984. Structural studies of plasma lipoproteins. *Basic Life Sci.* **27**: 211–226.
- Segrest, J. P., L. Li, G. M. Anantharamaiah, S. C. Harvey, K. N. Liadaki, and V. Zannis. 2000. Structure and function of apolipoprotein A-I and high-density lipoprotein. *Curr. Opin. Lipidol.* **11**: 105–115.
- Gursky, O. 2005. Apolipoprotein structure and dynamics. *Curr. Opin. Lipidol.* **16**: 287–294.
- Peters-Libeu, C. A., Y. Newhouse, D. M. Hatters, and K. H. Weisgraber. 2006. Model of biologically active apolipoprotein E bound to dipalmitoylphosphatidylcholine. *J. Biol. Chem.* **281**: 1073–1079.
- Morrow, J. A., K. S. Arnold, and K. H. Weisgraber. 1999. Functional characterization of apolipoprotein E isoforms overexpressed in *Escherichia coli*. *Protein Expr. Purif.* **16**: 224–230.
- Newhouse, Y., C. Peters-Libeu, and K. H. Weisgraber. 2005. Crystallization and preliminary x-ray diffraction analysis of apolipoprotein E-containing lipoprotein particles. *Acta Crystallogr. Sect. F Struct. Biol. Cryst. Commun.* **61**: 981–984.
- Saito, H., P. Dhanasekaran, D. Nguyen, P. Holvoet, S. Lund-Katz, and M. C. Phillips. 2003. Domain structure and lipid interaction in human apolipoproteins A-I and E, a general model. *J. Biol. Chem.* **278**: 23227–23232.
- Atkinson, D., H. M. Smith, J. Dickson, and J. P. Austin. 1976. Interaction of apoprotein from porcine high-density lipoprotein with dimyristoyl lecithin. 1. The structure of the complexes. *Eur. J. Biochem.* **64**: 541–547.
- Svergun, D. I. 1992. Determination of the regularization parameter in indirect-transform methods using perceptual criteria. *J. Appl. Crystallogr.* **25**: 495–503.
- Svergun, D. I., V. V. Volkov, M. B. Kozin, and H. B. Stuhmann. 1996. New developments in direct shape determination from small-angle scattering. 2. Uniqueness. *Acta Crystallogr. A.* **52**: 419–426.
- Svergun, D., C. Barberato, and M. H. J. Koch. 1995. CRY SOL—a program to evaluate x-ray solution scattering of biological macromolecules from atomic coordinates. *J. Appl. Crystallogr.* **28**: 768–773.
- Konarev, P. V., M. V. Petoukhov, and D. I. Svergun. 2001. MASSHA—a graphics system for rigid-body modelling of macromolecular complexes against solution scattering data. *J. Appl. Crystallogr.* **34**: 527–532.

29. Borhani, D. W., D. P. Rogers, J. A. Engler, and C. G. Brouillette. 1997. Crystal structure of truncated human apolipoprotein A-I suggests a lipid-bound conformation. *Proc. Natl. Acad. Sci. USA*. **94**: 12291–12296.
30. Feigin, L. A., and D. I. Svergun. 1987. *Structure Analysis by Small-Angle X-Ray and Neutron Scattering*. Plenum Press, New York.
31. Denisov, I. G., Y. V. Grinkova, A. A. Lazarides, and S. G. Sligar. 2004. Directed self-assembly of monodisperse phospholipid bilayer nanodiscs with controlled size. *J. Am. Chem. Soc.* **126**: 3477–3487.
32. Nagle, J. F., and S. Tristram-Nagle. 2000. Structure of lipid bilayers. *Biochim. Biophys. Acta*. **1469**: 159–195.
33. Moore, P. B., D. M. Engelman, and B. P. Schoenborn. 1974. Asymmetry in the 50S ribosomal subunit of *Escherichia coli*. *Proc. Natl. Acad. Sci. USA*. **71**: 172–176.
34. Hatters, D. M., C. A. Peters-Libeu, and K. H. Weisgraber. 2005. Engineering conformational destabilization into mouse apolipoprotein E. A model for a unique property of human apolipoprotein E4. *J. Biol. Chem.* **280**: 26477–26482.
35. Jayaraman, S., D. L. Gantz, and O. Gursky. 2004. Poly(ethylene glycol)-induced fusion and destabilization of human plasma high-density lipoproteins. *Biochemistry*. **43**: 5520–5531.
36. Cate, A., J. C. Patterson, M. K. Jones, W. G. Jerome, D. Bashtrykov, Z. Su, F. Gu, J. Chen, M. P. Aliste, S. C. Harvey, et al. 2006. Novel changes in discoidal high density lipoprotein morphology: a molecular dynamics study. *Biophys. J.* **90**: 4345–4360.
37. Schneeweis, L. A., V. Koppaka, S. Lund-Katz, M. C. Phillips, and P. H. Axelsen. 2005. Structural analysis of lipoprotein E particles. *Biochemistry*. **44**: 12525–12534.
38. King, J. L., and T. H. Jukes. 1969. Non-Darwinian evolution. *Science*. **164**: 788–798.
39. Shore, B., and V. Shore. 1974. An apolipoprotein preferentially enriched in cholesteryl ester-rich very low density lipoproteins. *Biochem. Biophys. Res. Commun.* **58**: 1–7.
40. Roque, A. C. A., and C. R. Lowe. 2005. Lessons from nature: on the molecular recognition elements of the phosphoprotein binding domains. *Biotechnol. Bioeng.* **91**: 546–555.
41. Segrest, J. P., R. L. Jackson, J. D. Morrisett, and A. M. Gotto, Jr. 1974. A molecular theory of lipid-protein interactions in the plasma lipoproteins. *FEBS Lett.* **38**: 247–253.
42. MacRaid, C. A., G. J. Howlett, and P. R. Gooley. 2004. The structure and interactions of human apolipoprotein C-II in dodecyl phosphocholine. *Biochemistry*. **43**: 8084–8093.
43. Getie, M., C. E. H. Schmelzer, and R. H. H. Neubert. 2005. Characterization of peptides resulting from digestion of human skin elastin with elastase. *Proteins*. **61**: 649–657.